

On the use of CHIME to Detect Long-Duration Radio Transients from Neutron Star Mergers

MINORI SHIKAUCHI,^{1,2} KIPP CANNON,² HAOXIANG LIN,³ TOMONORI TOTANI,^{3,2} AND J. RICHARD SHAW⁴

¹Department of Physics, the University of Tokyo, 7-3-1 Hongo, Bunkyo, Tokyo 113-0033, Japan

²Research Center for the Early Universe (RESCEU), the University of Tokyo, 7-3-1 Hongo, Bunkyo, Tokyo 113-0033, Japan

³Department of Astronomy, the University of Tokyo, 7-3-1 Hongo, Bunkyo, Tokyo 113-0033, Japan

⁴Department of Physics and Astronomy, University of British Columbia, 6224 Agricultural Road, Vancouver, BC V6T 1Z1, Canada

(Received July 20, 2021)

Submitted to ApJ

ABSTRACT

Short gamma-ray burst (SGRB) GRB170817A was found to be related to a binary neutron star (BNS) merger. It is uncertain whether all SGRBs are caused by BNS mergers, and also under what conditions a BNS merger can cause a SGRB. Search for long-duration afterglow from SGRBs in the radio band can reveal the details of the energy sources of SGRBs, the relativistic jet, and will provide important clues on their nature (Kasliwal et al. 2017). As BNS mergers can cause SGRBs, afterglow observations will also provide an alternative measurement of BNS merger rate independent of gravitational wave (GW) observations. In previous work by Feng et al. (2014), the feasibility of the detection of long-duration afterglows was considered using a variety of radio observatories and a simple flux threshold detection algorithm. Here, we consider a more sophisticated detection algorithm for SGRB afterglows, and provide an estimate of the trials factors for a realistic search to obtain an updated estimate for the possibility of observing afterglows with CHIME. Based on our detection algorithm, we estimate 751 afterglows per year can be detected using CHIME with 96 % of them off-axis, which are candidates for orphan afterglows. Our result predicts significantly fewer detectable sources per year than the earlier analysis (Feng et al. 2014), but confirms the essential conclusion that using CHIME to search for long-duration afterglows will be effective at constraining the astrophysical merger rate.

Keywords: stars: neutron — gamma rays: stars

1. INTRODUCTION

Gamma-ray bursts (GRBs) are extremely energetic events in the Universe. For short gamma-ray bursts (SGRBs), prompt emissions are short-duration, intense pulses that last shorter than ~ 2 seconds. There are 125 detections with SWIFT/Burst Alert Telescope ¹ so far. As time passes, long-lasting afterglows can be observed in the range of months to years, much longer than prompt emissions. They are very faint ranging from microjanskys to millijanskys. Among 125 detections, there are 83 afterglows detected in X-ray, 15 in UV/optical and only 6 in radio band. Afterglows in radio band are so faint that it is difficult to observe them.

GRB 170817A (Abbott et al. 2017a) is a SGRB detected with *Fermi*-GBM (Goldstein et al. 2017) and INTEGRAL (Savchenko et al. 2017), which arrived 1.7 s after GW 170817 (Abbott et al. 2017b), a gravitational wave (GW) from BNS merger. It is an unusual SGRB because it is much fainter than is typical (Connaughton et al. 2017; Goldstein et al. 2017; von Kienlin et al. 2017). In Kasliwal et al. (2017), there are some proposed models explaining fainter SGRBs. One is relativistic jet models with different observer angles. The other includes “cocoon”, that is, mildly relativistic matter outflow in addition to the former model. It is produced by a jet successfully breaking out BNS

Corresponding author: Minoru Shikauchi
 shikauchi@resceu.s.u-tokyo.ac.jp

¹ https://swift.gsfc.nasa.gov/archive/grb_table/

merger ejecta (successful jet) or failing to do that (choked jet) (Mooley et al. 2018; Nakar et al. 2018) or the fast tail of the dynamical merger ejecta (Mooley et al. 2018; Hotokezaka et al. 2018) initially driven by the shock wave formed at the collision front (Bauswein et al. 2013; Hotokezaka et al. 2013; Kyutoku et al. 2013; Kiuchi et al. 2017). After the observation of prompt emission, follow-up observations from UV to near-infrared wavelength took place and an electromagnetic counterpart SSS17a/AT2017gfo was observed (Arcavi et al. 2017; Chornock et al. 2017; Coulter et al. 2017; Cowperthwaite et al. 2017; Drout et al. 2017; Evans et al. 2017; Kasen et al. 2017; Kilpatrick et al. 2017; Pian et al. 2017; Savchenko et al. 2017; Shappee et al. 2017; Smartt et al. 2017; Tanaka et al. 2017; Tanvir et al. 2017; Valenti et al. 2017; Villar et al. 2017). The host galaxy of the counterpart is identified as NGC 4993, which is an elliptical galaxy with a luminosity distance of ~ 40 Mpc (Coulter et al. 2017). X-ray and radio emission was detected 9 and 16 days after the detection of GRB 170817A (Hallinan et al. 2017; Troja et al. 2017). Based on about 1 year observation, it turned out that the brightness changed $\propto t_{\text{obs}}^{0.8}$ (Resmi et al. 2018) and turned over after around 150 days (Dobie et al. 2018). Its spectrum follows a single and constant power-law spectral energy distribution $F_{\nu} \propto \nu^{-0.6}$ consistent with synchrotron radiation (Alexander et al. 2018; D'Avanzo et al. 2018; Dobie et al. 2018; Haggard et al. 2017; Hallinan et al. 2017; Lyman et al. 2018; Margutti et al. 2017, 2018; Mooley et al. 2018; Resmi et al. 2018; Troja et al. 2017; Troja et al. 2018; van Eerten 2018). However, the observed rising pattern challenges a homogeneous jet model or single-velocity spherical shell model of expanding ejecta because both models generate a faster rise in flux $F_{\nu} \propto t_{\text{obs}}^3$ (Mooley et al. 2018; Nakar & Piran 2018). Therefore, the homogeneous jet models are excluded and afterglow observations can help reveal the details of relativistic jet. There is another important implication from GRB 170817A. Since BNS merger can cause SGRB, afterglow observation will provide an alternative measurement of BNS merger rate independent of GW observations. Both BNS merger rate and SGRB event rate have been already measured (Abbott et al. 2017b; Fong et al. 2015), and afterglow observation will provide an upper limit of afterglow event rate, which has been never estimated. As there will be contamination from astrophysical phenomena with the same explosion mechanism such as Long GRB, we will only obtain the upper bound of the afterglow event rate.

The observed afterglows were so far detected in follow-up observations of prompt emissions. Outside of the jet opening angle, prompt emission is difficult to observe, but as time passes, the jet breaks and synchrotron emission occurs almost isotropically, and so an observer outside of the jet opening can observe this afterglow. Afterglow without observed prompt emission is called “orphan afterglow”. Rhoads (1997) indicated a number of SGRBs should be γ -ray faint, which can be observed as orphan afterglows. In addition, during the γ -ray emission phase, relativistic jets are highly beamed with Lorentz factor $\Gamma \sim 100$ (Fenimore et al. 1993; Woods & Loeb 1995). If the γ -ray emissions are beamed into a fraction f_b of the sky, f_b becomes $\sim \pi \Gamma^{-2} / 4\pi = 1/\Gamma^2$. While the Lorentz factor is ~ 100 during γ -ray emission phase, it decreases to of order unity when the radio afterglow emissions occur (Waxman et al. 1998). Therefore, a rate of observing radio afterglows is $\sim 10^4$ times larger than that of observing γ -ray emissions. Therefore, it is worth searching for orphan radio afterglows because it is more likely to observe radio afterglows than prompt emissions. Thanks to a small relativistic beaming effect, radio afterglow search will be effective at estimating the total energy and rate at which SGRBs occur precisely. Also, event rate of orphan afterglows depends on the structure of relativistic jet (Totani & Panaiteescu 2002; Nakar et al. 2002; Rossi et al. 2008). It would be helpful to give a constraint on the progenitor of SGRB. Some previous searches tried to observe orphan afterglows with small aperture telescopes (Grindlay 1999; Greiner et al. 2000; Rau et al. 2006; Malacrinò et al. 2007; Huang et al. 2020; Levinson et al. 2002; Gal-Yam et al. 2006), resulting in no confident detections.

The Canadian Hydrogen Intensity Mapping Experiment (CHIME) will greatly contribute to orphan afterglow searches with its wide instantaneous field of view of ~ 200 deg 2 . A previous work (Feng et al. 2014) theoretically estimated ~ 30 to 3000 orphan afterglows per year could be detected. CHIME is a cylindrical transit radio telescope located in British Columbia, Canada and thus observes the whole Northern sky one per day. It has four cylinders, each with 256×4 dual-polarization feeds and observes from 400 MHz to 800 MHz. At mid-band CHIME has an angular resolution of $0.22^\circ - 5.1^\circ \times 0.36^\circ$ depending on the declination (from projection effects the resolution is lower towards the local horizon). CHIME is designed for 21 cm line observation where synchrotron emission is a noise foreground that must be identified and be removed. Therefore, CHIME has synchrotron emission data in the Northern sky per a day. The CHIME simulation and data analysis pipeline is publicly available (CHIME Collaboration 2021a,b). With these you can simulate the response of the telescope to a simulated skymap. CHIME is expected to produce daily skymaps of the synchrotron amplitude everywhere in the northern sky.

In the event rate estimation of (Feng et al. 2014), they prepared a set of afterglow light curves using typical isotropic energies and circum medium densities. They assumed homogeneous jet model with fixed jet angle, 11.5° (0.2 rad),

a typical value, and the observer angle changes from 0° to 90° , on-axis to off-axis. However, the observation of GRB170817A, the only one event related to BNS merger, implied the existence of more complicated jet models. As our target is long-duration transients from BNS mergers to search for them we need to prepare light curve templates for complex jet SGRBs. To that end Lin et al. (2019) developed an excellent analytic calculation code for light curves from a relativistic jet with Gaussian energy profile, called “Gaussian jet model”, and (quasi-)spherical outflow with radially stratified velocity. In contrast to the previous efforts (D’Avanzo et al. 2018; Gill & Granot 2018; Hotokezaka et al. 2018; Margutti et al. 2018; Mooley et al. 2018; Nakar et al. 2018; Resmi et al. 2018; Troja et al. 2018) , they treat f , the number fraction of electrons injected to the shock acceleration process, and γ_m , the minimum Lorentz factor of electrons in the shock frame as free parameters. This treatment is effective if there are many light curve data points in a wide wavelength band. However, with few data points, the assumption that all the electrons in the shocked shell should be accelerated, that is $f = 1$, was adopted in the previous works (D’Avanzo et al. 2018; Gill & Granot 2018; Hotokezaka et al. 2018; Margutti et al. 2018; Mooley et al. 2018; Nakar et al. 2018; Resmi et al. 2018; Troja et al. 2018) , but this might be an oversimplification. It is more natural to think that some fraction of electrons remain as thermal particles as observed in supernova remnant (Laming 2001; Bamba et al. 2003). In addition to that they added some corrections and improvements to treat the radially stratified spherical model carefully. Therefore, in this work, we use the analytic calculation code of Lin et al. (2019). In Feng et al. (2014), they set two detection criteria for the prepared light curves. First, the peak flux of detectable light curve should be larger than a threshold value. Second, they define a duration of a light curve within which the flux is larger than half of the peak flux. Duration of detectable light curve should be shorter than 3 years. However, the event rates under the detection criteria might be overestimated because we cannot see such a clear light curve in a noisy data.

In this work, we employ a matched filtering technique (Helmstrom 1968) and likelihood ratio statistics (Neyman et al. 1933). In general, the sensitivity of a source-finding algorithm applied to each image is limited by non-thermal noise sources such as classical confusion noise caused by faint and unresolved background sources. If the instrumental resolution is improved, many unresolved sources can be resolved and the confusion noise will decrease. However, it is still critical for long observational time with source-finding algorithm. A simple way to find time-dependent sources is subtracting images taken at the same local sidereal time. Thanks to it, sidelobe confusion noise caused by residual synthesized beam sidelobes as well as classical confusion noise can be subtracted. However, for most surveys images are not taken at the same sidereal time each day, therefore, sidelobe confusion noise is large and image subtraction can be dominated by such artifacts. We have to treat these artifacts carefully because they can be identified as astrophysical transients (e.g. Frail et al. (2012) reported transient candidates Bower et al. (2007) found were artifacts or caused by calibration errors). Matched filtering technique Feng et al. (2017) employed is a method not only taking advantage of the nature of classical confusion noise without using source-finding algorithm that can limit the search sensitivity, but also using well-defined statistical properties including the distribution of the artifacts. Another previous work (Feng et al. 2017) adopted the likelihood ratio statistics to search for long-duration radio transients with the Murchison Widefield Array. In order to estimate the trials factor and set a detection threshold, they calculated a likelihood ratio for real data and fitted the distribution of likelihood ratio by assuming the negative log-likelihood ratio can be treated as an exponential function. Note that their survey is not dedicated to SGRB afterglow search, but for general long-duration transients. They used light curve templates with top-hat shape and fast rise and exponential decay.

In this paper, we employ the latest calculation code (Lin et al. 2019) for light curve templates reflecting the fact of GRB170817A. Also, we adopt the likelihood ratio statistic used in Feng et al. (2017) and develop an analytic estimate of trials factor in section 2. We show the results in section 3.3. We discuss the event rate of afterglows from SGRBs with CHIME in section 4. And, we conclude our analysis in section 5.

2. METHOD

The detection algorithm used here is based on likelihood ratio statistics. First, think of likelihood ratio Λ ,

$$\Lambda = \frac{P(\text{data}|\text{signal})}{P(\text{data}|\text{noise})}, \quad (1)$$

where $P(\text{data}|\text{signal})$ is a probability of obtaining a data set when a signal is included and $P(\text{data}|\text{noise})$ is that of obtaining a data set when no signals are included.

By generating mock data including only noise and calculating Λ , we can obtain $P(\ln \Lambda|\text{noise})$, a probability of obtaining Λ given only noise is included. If Λ is larger than a threshold value Λ_{th} , a signal can be detected with some

confidence level. Note that $P(\ln \Lambda | \text{noise})$ is the probability when comparing one pixel to one light curve template. Considering that CHIME's data is multi-pixel and we employed a suite of light curve templates, we can set Λ_{th} shown below,

$$P_{\text{exp}}(\ln \Lambda \geq \ln \Lambda_{\text{th}} | \text{noise}) < p, \quad (2)$$

where $P_{\text{exp}}(\ln \Lambda \geq \ln \Lambda_{\text{th}} | \text{noise})$ is a probability in “one experiment” of obtaining Λ larger than the threshold value Λ_{th} given only noises are included and p is “false alarm probability”. The value $P_{\text{exp}}(\ln \Lambda \geq \ln \Lambda_{\text{th}} | \text{noise})$ represents a probability of accidentally obtaining $\ln \Lambda$ larger than a threshold value $\ln \Lambda_{\text{th}}$ in one pixel at least. That can be calculated by subtracting a probability of obtaining $\ln \Lambda$ smaller than a threshold value $\ln \Lambda_{\text{th}}$ for all the pixels and statistically independent combinations of light curve templates. The meaning of “one experiment” is the full observation. We assumed one year observation at the band center, 600 MHz, for all the pixels.

As we will show later, Λ can be approximated like an inner product between data and a light curve template. The probability in one experiment $P_{\text{exp}}(\ln \Lambda \geq \ln \Lambda_{\text{th}} | \text{noise})$ can be calculated from that of one pixel and one light curve template $P(\ln \Lambda \geq \ln \Lambda_{\text{th}} | \text{noise})$,

$$P_{\text{exp}}(\ln \Lambda \geq \ln \Lambda_{\text{th}} | \text{noise}) = 1 - (1 - P(\ln \Lambda \geq \ln \Lambda_{\text{th}} | \text{noise}))^n, \quad (3)$$

where

$$n = n_{\text{pix}} \times n_{\text{dof}}, \quad (4)$$

n_{pix} is the number of independent pixels in an output image, 511×1409 and n_{dof} is D.O.F of light curve templates, the number of statistically independent light curve templates, 5. The value n_{dof} is estimated from singular-value decomposition (SVD), a matrix factorization that expands a matrix as a product of two orthogonal matrices and a diagonal matrix. By populating a matrix with many light curve templates, decomposing it using the SVD, and counting the number of non-zero elements in the diagonal matrix in the factorization, we see the number of orthogonal vectors that are needed to reconstruct any of the light curve templates. In our analysis, we generated $\sim 100,000$ light curve pieces with isotropic kinetic energy 10^{49} and 10^{51} ergs, circum medium density $10^{-5}, 10^{-3}$ and 1 cm^{-3} , observer angle $0 - 90^\circ$ with fixed jet opening angle 0.2 rad.

For each pixel in the output image, we assumed a data set x_i ($i = 1, 2, \dots, 365$) is a time-series of “pixel brightness”, which is obtained by converting visibility into an intrinsic flux in milli-Jansky. It includes two sources of noise: thermal noise σ_i and a constant background c from time-independent radio sources. Therefore, the data set can be expressed in two ways,

$$x_i = \sigma_i + c, \quad (5)$$

for Hypothesis 1: only noises are included in the data set, and

$$x_i = \sigma_i + c + Af_i. \quad (6)$$

where f_i is a light curve template we prepared and A is its amplitude for Hypothesis 2: a radio signal with a light curve f_i are included in the data set. Sidelobe confusion and time-dependence of thermal temperature will change σ_i , but, for simplicity, we considered only thermal noise and background contributor with its variance $\sigma^2 = (0.0232 \text{ mJy})^2$. The derivation is shown in Appendix B. We fixed the observed frequency as 600 MHz. The typical value of constant background is ~ 10 K, corresponding to 2.76 Jy / pixel. A duration of the full observation is assumed to be one year.

For Hypothesis 1, we assume white and stationary noise and the probability density function of a pixel brightness x_i , $p_i(x_i)$ becomes Gaussian distribution,

$$p_i(x_i) = \frac{1}{\sqrt{2\pi}\sigma_i} \exp\left[-\frac{(x_i - c)^2}{2\sigma_i^2}\right]. \quad (7)$$

Therefore, the numerator of likelihood ratio $P(\text{data} | \text{noise})$ can be expressed as

$$P(\text{data} | \text{noise}) = \prod_{i=1}^L p_i(x_i). \quad (8)$$

Also, for Hypothesis 2, the probability density function of a pixel brightness $p'_i(x_i)$ will change by a factor of Af_i ,

$$p'_i(x_i) = \frac{1}{\sqrt{2\pi}\sigma_i} \exp\left[-\frac{(x_i - c - Af_i)^2}{2\sigma_i^2}\right], \quad (9)$$

and we obtain $P(\text{data}|\text{signal})$,

$$P(\text{data}|\text{signal}) = \prod_{i=1}^L p'_i(x_i). \quad (10)$$

Now, we have two parameter, constant background c and signal amplitude A . With respect to them, we think about extremizing likelihood ratio. We have only to consider the exponents of $P(\text{data}|\text{noise})$ and $P(\text{data}|\text{signal})$, defined as χ_1^2 and χ_2^2 ,

$$\chi_1^2 = \sum_{i=1}^L \frac{(x_i - c)^2}{\sigma_i^2}, \quad (11)$$

$$\chi_2^2 = \sum_{i=1}^L \frac{(x_i - c - Af_i)^2}{\sigma_i^2}, \quad (12)$$

following the previous work (Feng et al. 2017).

$$\frac{\partial \chi_1^2}{\partial c} = - \sum_{i=1}^L \frac{2(x_i - c)}{\sigma_i^2} \quad (13)$$

For $\frac{\partial \chi_1^2}{\partial c} = 0$, we obtain

$$c_1 = \frac{\sum \frac{x_i}{\sigma_i^2}}{\sum \frac{1}{\sigma_i^2}} \equiv \langle \mathbf{x} \rangle, \quad (14)$$

$$\frac{\partial \chi_2^2}{\partial c} = - \sum_{i=1}^L \frac{2(x_i - c - Af_i)}{\sigma_i^2}, \quad \frac{\partial \chi_2^2}{\partial A} = - \sum_{i=1}^L \frac{2f_i(x_i - c - Af_i)}{\sigma_i^2} \quad (15)$$

For $\frac{\partial \chi_2^2}{\partial c}, \frac{\partial \chi_2^2}{\partial A} = 0$, we obtain

$$\begin{cases} \sum_{i=1}^L \frac{1}{\sigma_i^2} \langle \mathbf{f} \rangle A_2 + \sum_{i=1}^L \frac{1}{\sigma_i^2} c_2 = \sum_{i=1}^L \frac{1}{\sigma_i^2} \langle \mathbf{x} \rangle \\ (\mathbf{f}, \mathbf{f}) A_2 + \sum_{i=1}^L \frac{1}{\sigma_i^2} \langle \mathbf{f} \rangle c_2 = (\mathbf{x}, \mathbf{f}), \end{cases} \quad (16)$$

where

$$\langle \mathbf{x} \rangle \equiv \frac{\sum \frac{x_i}{\sigma_i^2}}{\sum \frac{1}{\sigma_i^2}}, \quad (\mathbf{x}, \mathbf{f}) \equiv \sum \frac{x_i f_i}{\sigma_i^2}, \quad (17)$$

and \sum represents summing up over days. Then, c_2 and A_2 , which extremize χ_2^2 , are expressed as

$$c_2 = \langle \mathbf{x} \rangle - A_2 \langle \mathbf{f} \rangle \quad (18)$$

$$A_2 = \frac{(\mathbf{x}, \mathbf{f}) - \sum_{i=1}^L \frac{1}{\sigma_i^2} \langle \mathbf{x} \rangle \langle \mathbf{f} \rangle}{(\mathbf{f}, \mathbf{f}) - \sum_{i=1}^L \frac{1}{\sigma_i^2} \langle \mathbf{f} \rangle^2} = \frac{(\mathbf{x}, \mathbf{f} - \langle \mathbf{f} \rangle)}{(\mathbf{f} - \langle \mathbf{f} \rangle, \mathbf{f} - \langle \mathbf{f} \rangle)}. \quad (19)$$

By substituting c_1, c_2 and A_2 into likelihood ratio, we obtain the maximum likelihood ratio Λ_{\max} ,

$$\ln \Lambda_{\max} = \frac{1}{2} \times \frac{(\mathbf{x}, \mathbf{f} - \langle \mathbf{f} \rangle)^2}{(\mathbf{f} - \langle \mathbf{f} \rangle, \mathbf{f} - \langle \mathbf{f} \rangle)}, \quad (20)$$

which is defined as $\rho^2/2\sigma_\rho^2$ in the previous work (Feng et al. 2017).

In order to estimate event rate, we prepared a bunch of light curve templates and distributed $\sim 400,000$ radio signals into space to calculate the fraction of detectable signals at fixed comoving distance. Note that the light curve templates are normalized at luminosity distance 40 Mpc. When it changes to d_L Mpc, the amplitude A will change by a factor of $(1+z) \times \left(\frac{40}{d_L}\right)^2$. We generated light curve templates by using an analytic calculation code (Lin et al. 2019). Since GRB170817A implies the more complicated jet structures, the code can calculate a light curve of an afterglow with it. The energy and Lorentz factor distribution within the relativistic jet is “Gaussian” jet model, with which both energy and Lorentz factor distributions are Gaussian distributions. We fixed jet opening angle to 0.2 rad. It is a typical value based on jet-break observations (Burrows et al. 2006; Soderberg et al. 2006; Fong et al. 2012, 2014). The intrinsic distribution of isotropic kinetic energy and circum medium density follows (Fong et al. 2015) with micro physics parameters $\epsilon_e = \epsilon_B = 0.1$, based on afterglow observations. We distributed simulated radio signals into space with the number of signals proportional to comoving distance squared up to 1500 Mpc. The real astrophysical cutoff of CHIME is unknown and the event rate depends on it. However, the distance cut-off in this work is large enough to discuss the event rate because the fraction of detectable signals at such a far distance is very small. The observer angle θ_{obs} is distributed in proportional to $\sin \theta_{\text{obs}}$ from $0 - 90^\circ$.

Based on the Monte-Carlo simulation, we obtain the fraction of detectable signals at comoving distance r , $P(\text{detection}|r)$,

$$P(\text{detection}|r) = P(\ln \Lambda \geq \ln \Lambda_{\text{th}} | \text{signal}) \times P(\text{not obscured}), \quad (21)$$

where $P(\text{not obscured})$ is a probability that a signal is not obscured by other sources. As the number of detectable sources increases, a signal is more likely to be obscured by other sources, which makes us difficult to observe it. The probability of a signal not obscured by other sources, $P(\text{not obscured})$, can be expressed by

$$P(\text{not obscured}) = \left(\frac{n_{\text{pix}} - 1}{n_{\text{pix}}} \right)^N, \quad (22)$$

where $(n_{\text{pix}} - 1)/n_{\text{pix}}$ is a probability that one of the other sources located closer than the signal do not occupy the pixel the signal exists, N is the number of sources located closer than the signal.

Assuming the progenitor of SGRBs is BNS merger, the event rate of SGRB afterglows N_{det} can be calculated by integrating $r^2 \times P(\text{detection}|r)$ up to 1500 Mpc,

$$N_{\text{det}} = R_{\text{BNS}} \times \frac{1}{2} \times 4\pi \int r^2 P(\text{detection}|r) dr. \quad (23)$$

The BNS merger rate is based on gravitational-wave observation (Abbott et al. 2020),

$$R_{\text{BNS}} = 980_{-730}^{+1490} \text{ Gpc}^{-3} \text{ yr}^{-1} \quad (24)$$

$$\text{upper limit} : 12600 \text{ Gpc}^{-3} \text{ yr}^{-1}. \quad (25)$$

Note that the factor 1/2 in (23) is based on the fact that CHIME observes all the Northern sky.

3. RESULT

3.1. Analytic Estimation of the Trials Factor

Here, we analytically estimate the trials factor $\ln \Lambda_{\text{th}}$. In Figure 1, blue histogram shows the distribution of Λ under Hypothesis 1: only noises are included in the data set of one pixel and one template, $P(\ln \Lambda | \text{noise})$. The orange line in the figure shows χ^2 distribution with one degree of freedom. In Wilks’ theorem Wilks (1938), $2 \ln \Lambda$ under Hypothesis 1 should follow χ^2 distribution with some D.O.F. Since the number of fitting parameters for $P(\text{data}|\text{signal})$ and $P(\text{data}|\text{noise})$ is 2 and 1 respectively, likelihood ratio should follow χ^2 distribution with one D.O.F. By using the χ^2 distribution, we calculated a probability of obtaining $\ln \Lambda$ larger than a threshold value $\ln \Lambda_{\text{th}}$ under Hypothesis 1, $P_{\text{exp}}(\ln \Lambda \geq \ln \Lambda_{\text{th}} | \text{noise})$, that is, “false alarm probability” (FAP). If FAP is small enough for a threshold value, a data set with larger likelihood ratio is considered as detectable. We set FAP as 0.1, namely that, one tenth of the data sets with larger likelihood ratio than the threshold is false positive. We call the detection threshold “90 % sample purity”. This FAP is small enough to discuss the event rate. BNS merger rate estimated from GW observation has three times uncertainty (Abbott et al. 2020). “90 % sample purity” corresponds to 10 % uncertainty of event rate estimation.

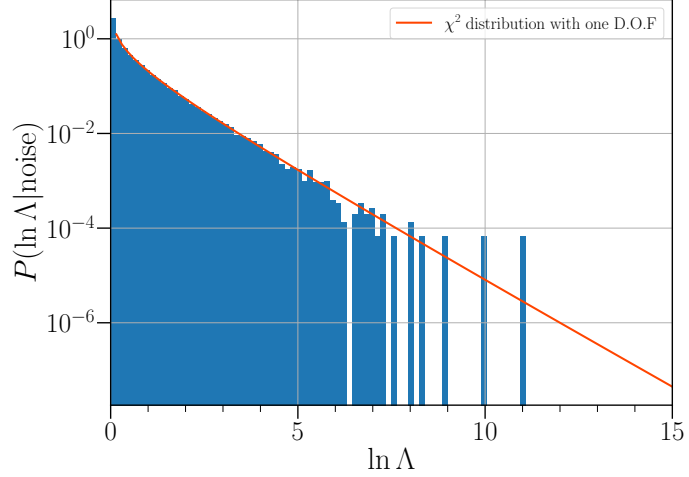


Figure 1. Distribution of $P(\ln \Lambda|\text{noise})$ in one pixel and one light curve template. It is obtained by generating random noise data and calculating $\ln \Lambda$. From Wilks' theorem Wilks (1938), it should follow χ^2 distribution and we confirmed χ^2 distribution with one D.O.F, orange line, matched our result. We employed the χ^2 distribution in order to calculate “false alarm probability” in one experiment.

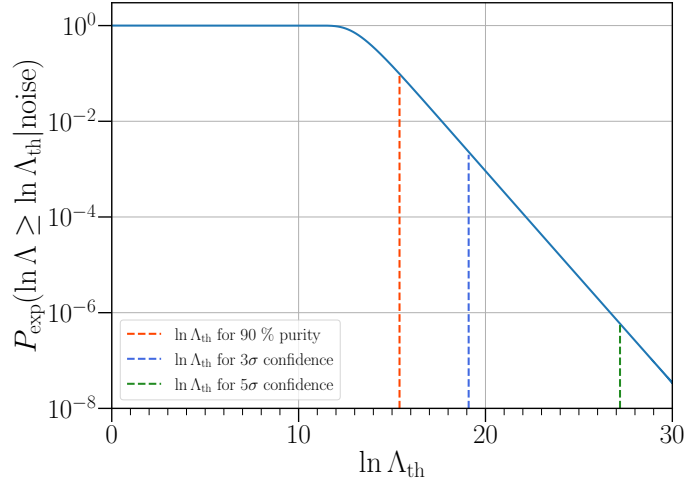


Figure 2. Distribution of a probability of obtaining $\ln \Lambda$ in one experiment given a data set only including noises, $P_{\text{exp}}(\ln \Lambda \geq \ln \Lambda_{\text{th}}|\text{noise})$, that is, “false alarm probability” (FAP). We set a threshold value for likelihood ratio, $\ln \Lambda_{\text{th}} = 15.4$ (red), for “90 % sample purity”. It means one tenth of data sets with likelihood ratio larger than the threshold should be false positive. This threshold is strict enough with respect to event rate estimation because 90 % sample purity causes 10 % uncertainty of event rate, smaller than that estimated in GW observation. For the comparison, we set thresholds corresponding to 3σ (blue) and 5σ confidence level (green), $\ln \Lambda_{\text{th}} = 19.1$ and 27.2 , respectively. As the threshold becomes stricter, the shape of a detectable signal gets clear in noisy data (see Figure 3).

It is stricter than estimated from GW observations. Figure 2 shows FAP calculated from the χ^2 distribution. The corresponding $\ln \Lambda_{\text{th}}$ for 90 % sample purity is 15.4.

Figure 3 shows examples of mock data including detectable signals with different detection thresholds, 90 % sample purity, 3σ and 5σ confidence levels. The blue lines are the mock data and the orange ones are the radio signals. As the threshold becomes stricter, the shape of detectable signal is significant.

3.2. Event Rate Estimation

To estimate the event rate we perform a Monte-Carlo simulation: generating a bunch of light curve templates, distributing them into space, and calculating the fraction of detectable signals at comoving distance r . Figure 4 shows the fraction of detectable signals at fixed comoving distance r , $p(\text{detection}|r)$. Blue histogram shows the distribution

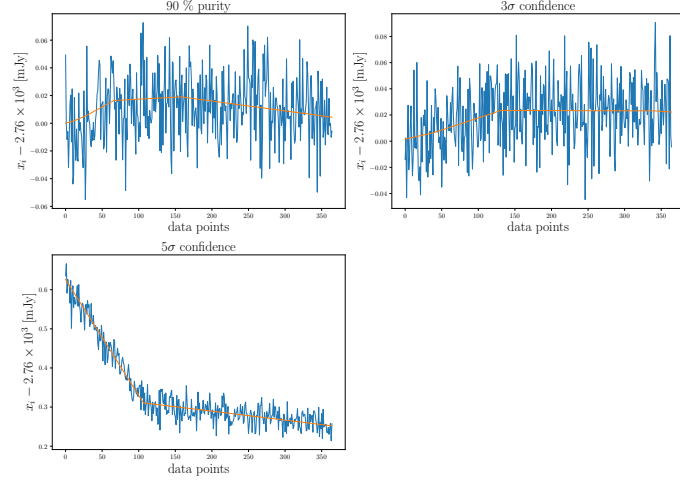


Figure 3. Examples of mock data. They include radio signals detectable with 90 % sample purity, 3σ and 5σ confidence levels. As the threshold becomes stricter, we can see the shape of a detectable signal in noisy data more clearly.

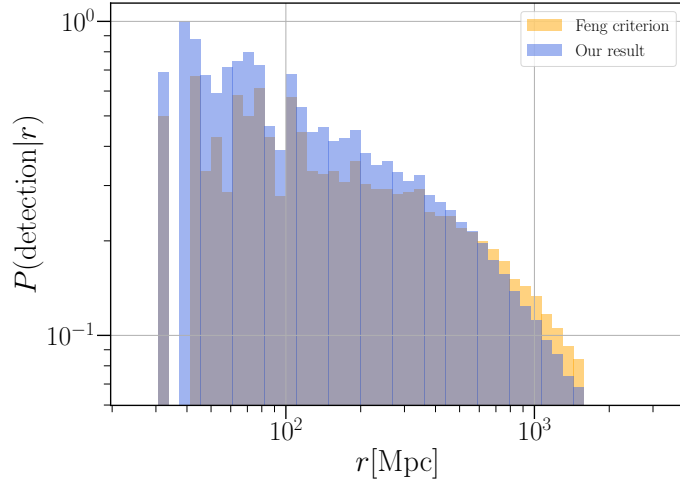


Figure 4. The probability that a signal located at comoving distance r [Mpc] can be detected. Blue histogram is based on the detection algorithm and orange one is based on the algorithm the previous work Feng et al. (2014) employed. By integrating the fractions, we obtained 751 year^{-1} and 857 year^{-1} SGRB afterglows can be detected with our criterion and Feng criterion respectively.

based on our detection criterion, 90 % sample purity. For the comparison, we calculated the fraction using detection criteria employed the previous work (Feng et al. 2014), the orange histogram called “Feng criterion”. The difference is a little significant for the farther sources. Feng criterion considered more radio signals can be detected. Since the number of signals increase by a factor of r^2 and the fraction decreases moderately, the difference affects the event rate estimation. Though our result estimated a larger fraction of signals can be detected for closer distance than 500 Mpc, but the contribution of such sources is negligible compared to that of farther sources. From the Monte-Carlo simulation, we estimated 751 year^{-1} SGRB afterglows can be detected with CHIME. Since the histogram is sparse at closer distance, we interpolate it so that the fraction of detectable signals at 0 Mpc is unity. This interpolation does not matter for event rate estimation because the number of signals is proportional to comoving distance squared and the signals located at farther distance is dominant for detectable ones. We summarized the event rate estimated based on our detection criterion and Feng criterion. The first line shows the result of Feng et al. (2014). They estimated the event rate with respect to circum medium density. By comparing the first line to the second one, the event rates are comparable. The third line, our result, is slightly smaller than the first and second lines. However, we confirmed the essential conclusion of the previous work, namely that, using CHIME to search for SGRB afterglows is effective.

	Event rate [year ⁻¹]			
	Pessimistic	Realistic	Optimistic	Upper limit
Feng et al. (2014)	8 – 750	29 – 2940	86 – 7410	504 – 25200
Feng criterion	220	857	2124	9707
Our result	193	751	1862	8568

Table 1. Event rate of SGRB afterglows. We estimated 751 year⁻¹ afterglows can be detected with CHIME. Our result estimated significantly smaller value than the previous work (Feng et al. 2014) estimated, but confirmed the essential conclusion of Feng et al. (2014): using CHIME to search for SGRB afterglows will be effective at constraining BNS merger rate.

3.3. Parameter Distribution of Detectable SGRB Afterglows

Here, we summarized the parameter distribution of SGRB afterglows considered as detectable. Figure 5 and 6 are the cumulative probability densities of isotropic kinetic energy and circum medium density. Blue histogram shows our result and orange one is the intrinsic distribution. For both distributions, our result is biased to larger value, corresponding to more energetic afterglows. That is because most of the detectable afterglows are off-axis ones. The distribution of observer angle is shown in Figure 7. 96 % of detectable afterglows have observer angle larger than the jet opening angle, $\theta_{\text{obs}} > \theta_{\text{jet}}$, that is, off-axis ones. The intrinsic distribution is based on on-axis afterglow observations. Since off-axis jet afterglows are fainter than on-axis ones, detectable off-axis afterglows should be energetic than detectable on-axis ones. Therefore, we obtained the parameter distribution biased to larger isotropic kinetic energy and circum medium density. Off-axis SGRBs are candidates for orphan afterglows, which implies that about 726 per year off-axis afterglows are detectable. Therefore, CHIME will be also effective at orphan afterglow search.

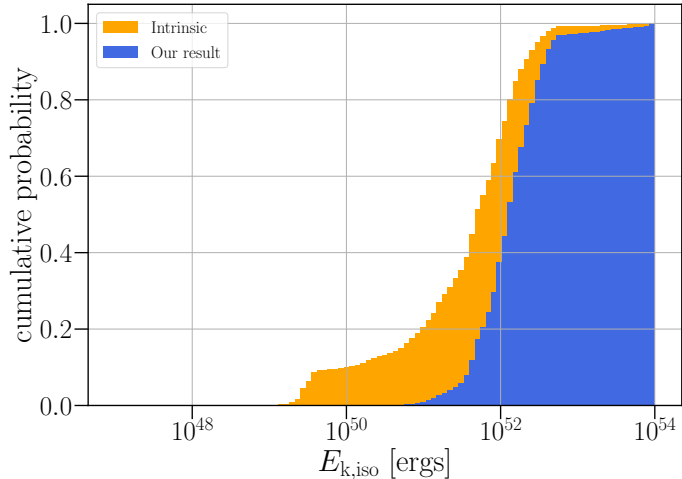


Figure 5. Cumulative density function of isotropic kinetic energy of detectable SGRBs. The distribution of isotropic kinetic energy of detectable signals (blue) is biased to larger value than the intrinsic distribution (orange).

4. DISCUSSION

Our result confirmed a significant number of afterglows can be detected with CHIME, 751 per year for 90 % sample purity. CHIME’s localization is a little robust and it is difficult to identify the candidates CHIME finds as SGRB afterglows or other transients such as long GRB afterglows and AGNs. However, CHIME will tell us the possible regions radio transients exist. By detecting a candidate by follow-up observation with other radio telescopes, we can determine its position. If they are elliptical galaxies and the sources are located far from their center, we can exclude the possibility of long GRBs and AGNs and conclude the candidates are real signals with high probability. It will lead us to discuss statistically the parameter distribution of relativistic jet such as jet opening angle by using a lot of samples. And also, from radio observation, we can estimate precise jet energy scales without considering relativistic effects. By determining the jet energy distribution formed by BNS mergers, we can give some constraints on BNS mergers as the progenitors of SGRBs: whether all the BNS mergers can cause SGRBs or some of them can. Our

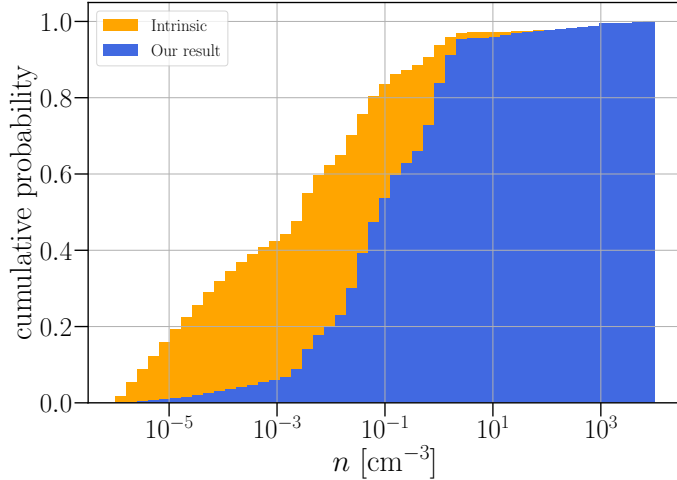


Figure 6. Cumulative density function of circum medium density of detectable SGRBs. The distribution of circum medium density of detectable signals (blue) is biased to larger value than the intrinsic distribution (orange).

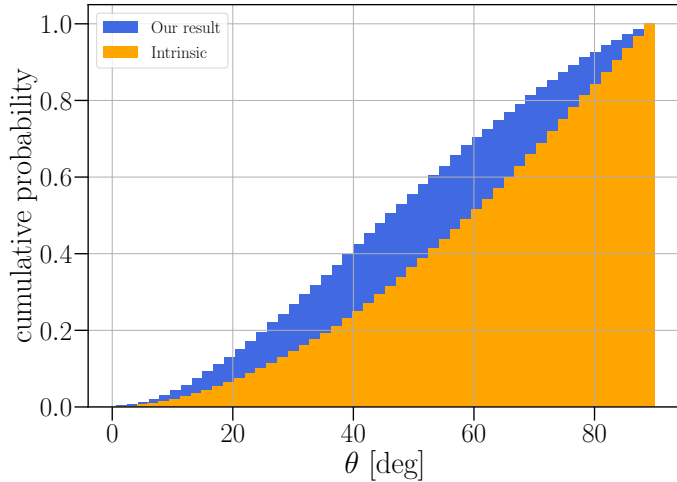


Figure 7. Cumulative density function of observer angle of detectable SGRBs. The distribution of observer angle of detectable signals (blue) is biased to smaller value than the intrinsic distribution (orange). Since 96 % of the detectable signals are off-axis jet afterglows and the intrinsic distribution is based on on-axis afterglow observation, detectable signals should be more energetic than on-axis afterglows, and therefore, the distributions of isotropic kinetic energy and circum medium density of detectable signals are biased to larger values.

analysis suggests the importance of using CHIME to estimate the afterglow event rate. When the observation with CHIME takes place, three event rates, BNS merger rate estimated by GW observation and SGRB event rate and afterglow event rate will be connected for the first time.

In this analysis, we fixed some parameters of relativistic jet such as jet opening angles. If we employ different value for the angles, the shape of afterglow light curves and their brightness will change. In addition to it, we fixed the relativistic jet model to Gaussian jet model. Jet model should also affect the afterglow light curves. Therefore, properties of relativistic jet might affect the event rate estimation. For the real analysis, we might be able to reverse the analysis and infer the physical properties of the detected afterglows after estimating afterglow event rate.

5. CONCLUSION

We employed a specific detection algorithm based on likelihood ratio statistics and developed an analytic estimate of the trials factor. We simulated the response of the detection algorithm to signals embedded in noises. Based on the result, we estimated a false alarm probability caused by the search over sky location and the choice of light curve templates. Taking all of that into consideration, we set a detection threshold based on target sample purity.

Considering thermal noise and a constant background contribution, we estimated 751, 193 at least, and 1862 at most afterglows per year can be detected at 600 MHz with CHIME in one year observation and 96 % of them are off-axis, which are candidates for orphan afterglows. Properties of relativistic jet would affect the event rate estimation. We can also infer the physical properties of the progenitor of detectable afterglows by reversing this analysis. Our more detailed analysis leads to the prediction of a smaller rate of detections, but it confirms the essential conclusion of the earlier analysis (Feng et al. 2014), namely that, using CHIME to search for SGRB afterglows will be effective at constraining the astrophysical merger rate as well as searching for orphan afterglow. Based on our analysis, we expect afterglow search with CHIME can drastically increase the number of samples and discuss statistically the parameter distribution of relativistic jet and we can give some constraints on BNS merger as the progenitor of SGRB.

In addition, our analysis indicates the importance of using CHIME to estimating afterglow event rate. Comparing BNS merger rate and SGRB event rate with the afterglow event rate should be helpful to identify the progenitor of SGRBs.

ACKNOWLEDGEMENT

Our work is supported by KAKENHI 18K03692 and 17H06362 and 20J12200.

APPENDIX

A. SINGULAR VALUE DECOMPOSITION (SVD)

We have a log-likelihood ratio ranking statistic, (20), that is computed using an expression of the form

$$\ln \Lambda \sim (\mathbf{x} \cdot \mathbf{f})^2 \quad (\text{A1})$$

where \mathbf{x} is a pixel time series and \mathbf{f} is a light curve template. We want to extremize $\ln \Lambda$ with respect to the family of functions to which \mathbf{f} belongs, and then estimate the probability of observing such a value in a data set consisting only of noise. We accomplish the extremization by computing $\ln \Lambda$ for many choices of \mathbf{f} and picking the highest value. As we compare the pixel time series to additional light curves, the significance of the match we will eventually identify is diminished for us having made many attempts to find it. To estimate the false-alarm probability we need to know how many statistically independent trials we will have conducted. Light curve templates, \mathbf{f} , that are very similar will produce similar values of $\ln \Lambda$; knowing one of the two $\ln \Lambda$ allows one to accurately guess the other, they are not truly statistically independent trials. What property of \mathbf{f} makes two of them statistically independent trials for $\ln \Lambda$? Assuming the pixel noise process to be stationary, white, and Gaussian, then when two light curves are orthogonal to each other, that is,

$$\mathbf{f}_1 \cdot \mathbf{f}_2 = 0, \quad (\text{A2})$$

then $\mathbf{x} \cdot \mathbf{f}_1$ and $\mathbf{x} \cdot \mathbf{f}_2$ are uncorrelated. Since they are also Gaussian random variables they are statistically independent, and therefore the $\ln \Lambda$ computed for orthogonal light curves are statistically independent. Conversely, if $\mathbf{f}_1 \cdot \mathbf{f}_2 \neq 0$ then the $\ln \Lambda$ computed for them are not statistically independent.

The number of mutually orthogonal functions that can be found in the family of light curves tells us how many statistically independent values of $\ln \Lambda$ can be computed from that family of functions; the $\ln \Lambda$ for any other light curve can be computed from a combination of those $\ln \Lambda$ without any need to consult the data. We find this number by first assembling a matrix whose rows consist of light curve functions and then estimating the rank of the span of that matrix. The matrix we constructed contained $\sim 100,000$ one-year long light curve fragments with isotropic kinetic energy between 10^{49} erg and 10^{51} erg, circum medium density 10^{-5} cm^{-3} , 10^{-3} cm^{-3} , and 1 cm^{-3} , observer angle 0° – 90° with fixed jet opening angle 0.2 rad. Next we estimate the rank of the span of that matrix using a singular value decomposition (SVD). The SVD factors a matrix into a product of two orthogonal matrices and a diagonal matrix of singular values. The number of non-zero singular values gives the rank of the span of the original matrix.

When doing this, typically no singular values are found to be identically zero, but they will often be found to be either “large” or “small”, with many orders of magnitude between the two. An approximation of the original matrix can be obtained by replacing some number of the smallest singular values with 0s. The vectors corresponding to the non-zero singular values that remain provide the orthonormal basis of that rank that best approximates the rows in the original matrix in the sum of square residuals sense (this is a defining property of the SVD). By setting all “small”

singular values to 0, and retaining the “large”, we obtain a sensible approximation of the light curves, and the number of singular values we retain tells us exactly the rank of the space spanned by that approximation. We use this for n_{dof} when estimating the false-alarm probability.

This procedure is not a rigorous derivation of the distribution of $\ln \Lambda$ extremized over the template bank, and the method by which we extract n_{dof} by counting “large” singular values is ad hoc. However, the event rate is quite insensitive to the number of degrees of freedom, n_{dof} : we find that changing the estimate of this parameter by an order of magnitude in either direction changes the final estimated detectable event rate by less than 5%. Therefore, any sensible estimate within one or two orders of magnitude of the correct trials factor is adequate.

B. NOISE LEVEL ESTIMATION

Here, we introduce how we derive the variance caused by antenna receiver and unresolved background sources.

First, we assume CHIME has a receiver temperature of 50 K and the sky contributes around 10 K. The contribution of noise σ can be calculated following Equation (B5) in Feng et al. (2014),

$$\sigma = \left(\frac{2k_{\text{B}}T}{A_{\text{eff}}N_{\text{ant,tot}}\epsilon_c} \right) \frac{1}{\sqrt{N_{\text{pol}}Bt_{\text{int}}(\delta)}}, \quad (\text{B3})$$

where T is a noise temperature caused by antenna receiver and the background contributor of each antenna feed, A_{eff} is an effective antenna area of each feed, $N_{\text{ant,tot}}$ is the number of all the antenna feeds of CHIME, ϵ_c is a correlator efficiency, N_{pol} is the number of polarizations, B is the instantaneous bandwidth, and $t_{\text{int}}(\delta)$ is an integration time depending on the source declination δ . Here, we set $T = 60$ K, $\epsilon_c = 1.0$, $N_{\text{pol}} = 2$, $B = 400$ MHz, $A_{\text{eff}}N_{\text{ant,tot}} = 10000$ m². For t_{int} , following Feng et al. (2014),

$$t_{\text{int}}(\delta) = \frac{1}{2\pi} \arccos \left[\frac{-\sin^2 \delta + \cos \Delta \cos^2(\phi - \delta) + \sin^2(\phi - \delta)}{\cos^2 \delta} \right], \quad (\text{B4})$$

where $\Delta = 2.5^\circ$ and $\phi = 49^\circ$. Note that if a radio source is located at $\delta < \phi$, we will observe it once a day. Otherwise, if it is located at $\delta > \phi$, we can observe it twice a day. For that case, the integration time t_{int} can be expressed as

$$t_{\text{int}}(\delta) = \frac{1}{2\pi} \left[\arccos \left(\frac{-\sin^2 \delta + \cos \Delta \cos^2(\phi - \delta) + \sin^2(\phi - \delta)}{\cos^2 \delta} \right) + \arccos \left(\frac{-\sin^2 \delta + \cos \Delta \cos^2(\phi + \delta) + \sin^2(\phi + \delta)}{\cos^2 \delta} \right) \right]. \quad (\text{B5})$$

The second term of the equation includes the effect of the second transit of the source. Averaging over the declination $0^\circ \leq \delta \leq 90^\circ$, we obtain the noise flux thorough one day observation $\langle \sigma \rangle$,

$$\langle \sigma \rangle = 0.0232 \text{ mJy}. \quad (\text{B6})$$

By substituting $T = 50$ K for (B3), we obtain an average thermal noise variance $\langle \sigma_{\text{th}} \rangle$,

$$\langle \sigma_{\text{th}} \rangle = 0.0193 \text{ mJy}. \quad (\text{B7})$$

It is used for calculating the event rate based on Feng criterion.

REFERENCES

Abbott, B. P., et al. 2017a, ApJL, 848, L13, doi: [10.3847/2041-8213/aa920c](https://doi.org/10.3847/2041-8213/aa920c)
—. 2017b, PhRvL, 119, 161101, doi: [10.1103/PhysRevLett.119.161101](https://doi.org/10.1103/PhysRevLett.119.161101)
—. 2020, ApJL, 892, L3, doi: [10.3847/2041-8213/ab75f5](https://doi.org/10.3847/2041-8213/ab75f5)
Alexander, K. D., et al. 2018, ApJL, 863, L18, doi: [10.3847/2041-8213/aad637](https://doi.org/10.3847/2041-8213/aad637)
Arcavi, I., et al. 2017, Nature, 551, 64, doi: [10.1038/nature24291](https://doi.org/10.1038/nature24291)
Bamba, A., Yamazaki, R., Ueno, M., & Koyama, K. 2003, ApJ, 589, 827, doi: [10.1086/374687](https://doi.org/10.1086/374687)
Bauswein, A., Goriely, S., & Janka, H. T. 2013, ApJ, 773, 78, doi: [10.1088/0004-637X/773/1/78](https://doi.org/10.1088/0004-637X/773/1/78)

Bower, G. C., Saul, D., Bloom, J. S., et al. 2007, *ApJ*, 666, 346, doi: [10.1086/519831](https://doi.org/10.1086/519831)

Burrows, D. N., et al. 2006, *ApJ*, 653, 468, doi: [10.1086/508740](https://doi.org/10.1086/508740)

CHIME Collaboration. 2021a, Radio Cosmology, <https://github.com/radiocosmology/>

—. 2021b, CHIME, <https://github.com/chime-experiment/>

Chornock, R., et al. 2017, *ApJL*, 848, L19, doi: [10.3847/2041-8213/aa905c](https://doi.org/10.3847/2041-8213/aa905c)

Connaughton, V., et al. 2017, GRB Coordinates Network, 21506, 1

Coulter, D. A., et al. 2017, *Science*, 358, 1556, doi: [10.1126/science.aap9811](https://doi.org/10.1126/science.aap9811)

Cowperthwaite, P. S., et al. 2017, *ApJL*, 848, L17, doi: [10.3847/2041-8213/aa8fc7](https://doi.org/10.3847/2041-8213/aa8fc7)

D'Avanzo, P., et al. 2018, *A&A*, 613, L1, doi: [10.1051/0004-6361/201832664](https://doi.org/10.1051/0004-6361/201832664)

Dobie, D., et al. 2018, *ApJL*, 858, L15, doi: [10.3847/2041-8213/aac105](https://doi.org/10.3847/2041-8213/aac105)

Drout, M. R., et al. 2017, *Science*, 358, 1570, doi: [10.1126/science.aaq0049](https://doi.org/10.1126/science.aaq0049)

Evans, P. A., et al. 2017, *Science*, 358, 1565, doi: [10.1126/science.aap9580](https://doi.org/10.1126/science.aap9580)

Feng, L., Vaulin, R., & Hewitt, J. 2014, <https://arxiv.org/abs/arXiv:1405.6219>

Feng, L., et al. 2017, *AJ*, 153, 98, doi: [10.3847/1538-3881/153/3/98](https://doi.org/10.3847/1538-3881/153/3/98)

Fenimore, E. E., Epstein, R. I., & Ho, C. 1993, *A&AS*, 97, 59

Fong, W., Berger, E., Margutti, R., & Zauderer, B. A. 2015, *The Astrophysical Journal Letters*, 815, 102, doi: [10.1088/0004-637X/815/2/102](https://doi.org/10.1088/0004-637X/815/2/102)

Fong, W., et al. 2012, *ApJ*, 756, 189, doi: [10.1088/0004-637X/756/2/189](https://doi.org/10.1088/0004-637X/756/2/189)

—. 2014, *ApJ*, 780, 118, doi: [10.1088/0004-637X/780/2/118](https://doi.org/10.1088/0004-637X/780/2/118)

Frail, D. A., Kulkarni, S. R., Ofek, E. O., Bower, G. C., & Nakar, E. 2012, *ApJ*, 747, 70, doi: [10.1088/0004-637X/747/1/70](https://doi.org/10.1088/0004-637X/747/1/70)

Gal-Yam, A., Ofek, E. O., Poznanski, D., et al. 2006, *ApJ*, 639, 331, doi: [10.1086/499157](https://doi.org/10.1086/499157)

Gill, R., & Granot, J. 2018, *MNRAS*, 478, 4128, doi: [10.1093/mnras/sty1214](https://doi.org/10.1093/mnras/sty1214)

Goldstein, A., et al. 2017, *The Astrophysical Journal*, 848, L14, doi: [10.3847/2041-8213/aa8f41](https://doi.org/10.3847/2041-8213/aa8f41)

Goldstein, A., et al. 2017, GRB Coordinates Network, 21528, 1

Greiner, J., Hartmann, D. H., Voges, W., et al. 2000, *A&A*, 353, 998. <https://arxiv.org/abs/astro-ph/9910300>

Grindlay, J. E. 1999, *ApJ*, 510, 710, doi: [10.1086/306617](https://doi.org/10.1086/306617)

Haggard, D., et al. 2017, *ApJL*, 848, L25, doi: [10.3847/2041-8213/aa8ede](https://doi.org/10.3847/2041-8213/aa8ede)

Hallinan, G., et al. 2017, *Science*, 358, 1579, doi: [10.1126/science.aap9855](https://doi.org/10.1126/science.aap9855)

Helmstrom, C. W. 1968, *Statistical Theory of Signal Detection* (2nd ed.)

Hotokezaka, K., Kiuchi, K., Kyutoku, K., et al. 2013, *Phys. Rev. D*, 87, 024001, doi: [10.1103/PhysRevD.87.024001](https://doi.org/10.1103/PhysRevD.87.024001)

Hotokezaka, K., et al. 2018, *The Astrophysical Journal*, 867, 95, doi: [10.3847/1538-4357/aadf92](https://doi.org/10.3847/1538-4357/aadf92)

Huang, Y.-J., et al. 2020, *ApJ*, 897, 69, doi: [10.3847/1538-4357/ab8f9a](https://doi.org/10.3847/1538-4357/ab8f9a)

Kasen, D., et al. 2017, *Nature*, 551, 80, doi: [10.1038/nature24453](https://doi.org/10.1038/nature24453)

Kasliwal, M. M., et al. 2017, *Science*, 358, 1559, doi: [10.1126/science.aap9455](https://doi.org/10.1126/science.aap9455)

Kilpatrick, C. D., et al. 2017, *Science*, 358, 1583, doi: [10.1126/science.aaq0073](https://doi.org/10.1126/science.aaq0073)

Kiuchi, K., et al. 2017, *Phys. Rev. D*, 96, 084060, doi: [10.1103/PhysRevD.96.084060](https://doi.org/10.1103/PhysRevD.96.084060)

Kyutoku, K., Ioka, K., & Shibata, M. 2013, *Monthly Notices of the Royal Astronomical Society: Letters*, 437, L6, doi: [10.1093/mnrasl/slt128](https://doi.org/10.1093/mnrasl/slt128)

Laming, J. M. 2001, *ApJ*, 546, 1149, doi: [10.1086/318317](https://doi.org/10.1086/318317)

Levinson, A., Ofek, E. O., Waxman, E., & Gal-Yam, A. 2002, *ApJ*, 576, 923, doi: [10.1086/341866](https://doi.org/10.1086/341866)

Lin, H., Totani, T., & Kiuchi, K. 2019, *Monthly Notices of the Royal Astronomical Society*, 485, 2155, doi: [10.1093/mnras/stz453](https://doi.org/10.1093/mnras/stz453)

Lyman, J. D., et al. 2018, *Nature Astronomy*, 2, 751, doi: [10.1038/s41550-018-0511-3](https://doi.org/10.1038/s41550-018-0511-3)

Malacrinò, F., Atteia, J. L., Boér, M., et al. 2007, *A&A*, 464, L29, doi: [10.1051/0004-6361:20066912](https://doi.org/10.1051/0004-6361:20066912)

Margutti, R., et al. 2017, *ApJL*, 848, L20, doi: [10.3847/2041-8213/aa9057](https://doi.org/10.3847/2041-8213/aa9057)

—. 2018, *ApJL*, 856, L18, doi: [10.3847/2041-8213/aab2ad](https://doi.org/10.3847/2041-8213/aab2ad)

Mooley, K. P., et al. 2018, *Nature*, 554, 207, doi: [10.1038/nature25452](https://doi.org/10.1038/nature25452)

Nakar, E., & Piran, T. 2018, *Monthly Notices of the Royal Astronomical Society*, 478, 407, doi: [10.1093/mnras/sty952](https://doi.org/10.1093/mnras/sty952)

Nakar, E., Piran, T., & Granot, J. 2002, *ApJ*, 579, 699, doi: [10.1086/342791](https://doi.org/10.1086/342791)

Nakar, E., et al. 2018, *The Astrophysical Journal*, 867, 18, doi: [10.3847/1538-4357/aae205](https://doi.org/10.3847/1538-4357/aae205)

Neyman, J., Pearson, E. S., & Pearson, K. 1933, *Philosophical Transactions of the Royal Society of London. Series A, Containing Papers of a Mathematical or Physical Character*, 231, 289, doi: [10.1098/rsta.1933.0009](https://doi.org/10.1098/rsta.1933.0009)

Pian, E., et al. 2017, *Nature*, 551, 67, doi: [10.1038/nature24298](https://doi.org/10.1038/nature24298)

Rau, A., Greiner, J., & Schwarz, R. 2006, *A&A*, 449, 79, doi: [10.1051/0004-6361:20054317](https://doi.org/10.1051/0004-6361:20054317)

Resmi, L., et al. 2018, *ApJ*, 867, 57, doi: [10.3847/1538-4357/aae1a6](https://doi.org/10.3847/1538-4357/aae1a6)

Rhoads, J. E. 1997, *ApJL*, 487, L1, doi: [10.1086/310876](https://doi.org/10.1086/310876)

Rossi, E. M., Perna, R., & Daigne, F. 2008, *MNRAS*, 390, 675, doi: [10.1111/j.1365-2966.2008.13736.x](https://doi.org/10.1111/j.1365-2966.2008.13736.x)

Savchenko, V., et al. 2017, *The Astrophysical Journal*, 848, L15, doi: [10.3847/2041-8213/aa8f94](https://doi.org/10.3847/2041-8213/aa8f94)

Shappee, B. J., et al. 2017, *Science*, 358, 1574, doi: [10.1126/science.aaq0186](https://doi.org/10.1126/science.aaq0186)

Smartt, S. J., et al. 2017, *Nature*, 551, 75, doi: [10.1038/nature24303](https://doi.org/10.1038/nature24303)

Soderberg, A. M., et al. 2006, *ApJ*, 650, 261, doi: [10.1086/506429](https://doi.org/10.1086/506429)

Tanaka, M., et al. 2017, *Publications of the Astronomical Society of Japan*, 69, doi: [10.1093/pasj/psx121](https://doi.org/10.1093/pasj/psx121)

Tanvir, N. R., et al. 2017, *ApJL*, 848, L27, doi: [10.3847/2041-8213/aa90b6](https://doi.org/10.3847/2041-8213/aa90b6)

Totani, T., & Panaiteescu, A. 2002, *ApJ*, 576, 120, doi: [10.1086/341738](https://doi.org/10.1086/341738)

Troja, E., et al. 2017, *Nature*, 551, 71, doi: [10.1038/nature24290](https://doi.org/10.1038/nature24290)

Troja, E., Piro, L., Ryan, G., et al. 2018, *Monthly Notices of the Royal Astronomical Society: Letters*, 478, L18, doi: [10.1093/mnrasl/sly061](https://doi.org/10.1093/mnrasl/sly061)

Valenti, S., et al. 2017, *ApJL*, 848, L24, doi: [10.3847/2041-8213/aa8edf](https://doi.org/10.3847/2041-8213/aa8edf)

van Eerten, H. J. 2018, *arXiv e-prints*, arXiv:1808.10718. <https://arxiv.org/abs/1808.10718>

Villar, V. A., et al. 2017, *ApJL*, 851, L21, doi: [10.3847/2041-8213/aa9c84](https://doi.org/10.3847/2041-8213/aa9c84)

von Kienlin, A., Meegan, C., & Goldstein, A. 2017, *GRB Coordinates Network*, 21520, 1

Waxman, E., Kulkarni, S. R., & Frail, D. A. 1998, *ApJ*, 497, 288, doi: [10.1086/305467](https://doi.org/10.1086/305467)

Wilks, S. S. 1938, *Ann. Math. Statist.*, 9, 60, doi: [10.1214/aoms/1177732360](https://doi.org/10.1214/aoms/1177732360)

Woods, E., & Loeb, A. 1995, *ApJ*, 453, 583, doi: [10.1086/176421](https://doi.org/10.1086/176421)